GEOMETRIC MECHANICS, DYNAMICS, AND CONTROL OF FISHLIKE SWIMMING IN A PLANAR IDEAL FLUID

SCOTT DAVID KELLY*, PARTHESH PUJARI†, AND HAILONG XIONG‡

Abstract. We summarize the geometric treatment of locomotion in an ideal fluid in the absence of vorticity and link this work to a planar model incorporating localized vortex shedding evocative of vortex shedding from the caudal fin of a swimming fish. We present simulations of open-loop and closed-loop navigation and energy-harvesting by a Joukowski foil with variable camber shedding discrete vorticity from its trailing tip.

Key words. Geometric mechanics, vortex dynamics, locomotion.

AMS(MOS) subject classifications. Primary 70H33, 76B47, 93C10

1. Introduction. In this paper, we present an idealized model for planar fishlike swimming and explore the dynamics and control of this model. The model represents the synthesis of two lines of research pertaining to ideal hydrodynamics, one addressing the locomotion of free deformable bodies in the absence of vorticity and the other addressing the interaction of free rigid bodies with systems of discrete vorticity. The paper begins with a survey of concepts arising in this earlier work, focused in particular on the realization of locomotion problems in terms of analytical mechanics and nonlinear control systems on differentiable manifolds. The latter sections of the paper focus on the computational study of idealized fishlike swimming with an eye toward simple feedback control design for navigation and energy harvesting.

2. The Geometric View of Locomotion. A mathematical framework for modeling the locomotion of a deformable body can be derived from the geometry of the space in which the variables parametrizing the problem reside. Implicit in the following discussion are the smoothness assumptions needed to justify our regarding this space and various subspaces thereof as differentiable manifolds. The material that follows has been addressed in mathematical detail elsewhere [4]; we endeavor to summarize the essential concepts with only as much detail as is needed for practical calculations.

2.1. Configuration Space as a Principal Fiber Bundle. We refer to a time-parametrized curve in a manifold as a *trajectory* and the image of this curve — in other words, the sequential locus of points it comprises,

*Department of Mechanical Engineering and Engineering Science, University of North Carolina at Charlotte, Charlotte, North Carolina 28205.

†Department of Mechanical Engineering and Engineering Science, University of North Carolina at Charlotte, Charlotte, North Carolina 28205.

‡Quantitative Risk Management, Inc., Chicago, Illinois 60602. The work of all three authors was supported in part by NSF grant CMMI 04-49319.

without regard to time parametrization — as a *path*. We regard the instantaneous shape of a deformable body — distinct from its position or orientation relative to a frame of reference affixed to its environment — as corresponding to a point in a *shape manifold*. We assume that a body changing shape for the sake of locomotion has direct authority over its trajectory in its shape manifold; we forego analysis of the forces or moments needed to assert this authority. Our focus will be the manner in which prescribed changes in shape generate locomotion. We refer to a periodic change in a body's shape, corresponding to a closed path in the shape manifold, as a *gait*. The variability in a body's shape may be infinite-dimensional, but the concrete examples we describe will focus on bodies with finitely many internal degrees of freedom, and for simplicity's sake we will assume a finite-dimensional shape manifold for the remainder of the discussion. We use the symbol M to denote a body's shape manifold and the symbol r to denote a point in M corresponding to a particular shape.

As a rigid body moves through ambient space, its position and orientation may be specified relative to a reference configuration, perhaps corresponding to the body's position and orientation at some initial time. In the case of a deformable body, such a comparison requires that a method be specified for affixing a preferred frame of reference to the body — henceforth the *body frame* — in each of its different shapes. With such a method in place, we may identify each position and orientation of a deformable body with an element of a Lie group G of rigid motions relative to the body's reference configuration. In general, this group is the Euclidean group $SE(3)$ comprising displacements and rotations in three spatial dimensions, but certain locomotion problems require only strict Lie subgroups of $SE(3)$ to be considered. We will describe problems in planar locomotion for which $G = SE(2)$ and problems in rectilinear locomotion for which $G = (\mathbb{R}, +)$. In every case, we use the symbol g to denote an arbitrary element in the relevant group G, and the symbol e to denote the identity element associated with the reference configuration.

The locomotion of a deforming body may thus be described in terms of a trajectory in $M \times G$, resulting from dynamics influenced by the prespecified projection of this trajectory into M alone. It may be the case that the path in M is sufficient to determine the corresponding path in $M \times G$, or it may not. It may be the case that coordinates on $M \times G$, together with their time derivatives, furnish sufficiently many variables to model the governing dynamics, or it may not. In particular, when a deforming body swims through a fluid, additional variables are generally needed to represent the dynamics of the fluid. Only under special circumstances is the evolution of a fluid determined uniquely by the motion of a body through it, obviating — or formally eliminating via dynamic *reduction* [9] — additional variables to represent the fluid's internal degrees of freedom. Section 2.3 examines the locomotion of deforming bodies through irrotational ideal flows and through Stokes flows, representing precisely these special circumstances.

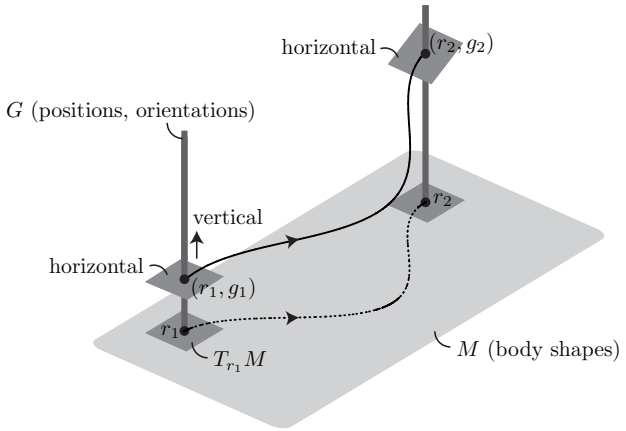

FIG. 1. *A principal fiber bundle $M \times G$. The base manifold M is shown with two dimensions and the group G with one. A connection defines a horizontal subspace of each tangent space $T_{(r,g)}(M \times G)$, isomorphic to the tangent space $T_r M$ and complementary to the vertical subspace of $T_{(r,g)}(M \times G)$. The curve in M passing through r_1 has a unique horizontal lift passing through (r_1, g_1).*

Section 3 summarizes a model in which a finite collection of point vortices is used to represent additional degrees of freedom in the fluid surrounding a planar swimmer.

The product $M \times G$ may be regarded as a fiber bundle over M. Each base point corresponds to a particular body shape; the points comprising the fiber over this base point represent the various ways of situating and orienting the body in its environment. Since G is a Lie group, the bundle over M is a *principal bundle* [7], accommodating the constructions defined below.

2.2. Principal Connections and Driftless Locomotion. A *connection* on the principal fiber bundle $M \times G$ specifies a manner in which a path in M passing through the point r may be identified with a unique path in $M \times G$ passing through a given point in the fiber over r. A connection corresponds to a splitting of the tangent space at each point in $M \times G$ into *horizontal* and *vertical* subspaces. The horizontal subspace at each point in the fiber over r is isomorphic to $T_r M$. The vertical subspace has dimension equal to the dimension of G; identifying $T_{(r,g)}(M \times G)$ with $T_r M \times T_g G$ we regard the vertical subspace as comprising vectors in $T_r M \times T_g G$ of the form $(0, \cdot)$. See Figure 1.

A trajectory in $M \times G$ is said to be horizontal relative to a given connection if every vector tangent to the trajectory is horizontal. A *horizontal lift* of a trajectory in M is a horizontal trajectory in $M \times G$ that projects onto the trajectory in M. If two trajectories in M correspond to the same path — in other words, they differ only in their time-parameterizations —

then they will lift to the same set of paths in $M \times G$.

In the context of locomotion, a connection specifies a unique mapping between sequential shape changes and sequential translations and reorientations. A connection completely models the relationship between shape change and locomotion only if the underlying dynamics involve no variables other than coordinates on M and G, and only if the rate at which a body changes shape has no bearing on the body's resulting motion through space. A system that satisfies these criteria may be termed *kinematic*.

In practice, a connection is typically specified by defining a one-form on M called the *local connection form*. In a manner that may vary from point to point in M, the local connection form maps vectors tangent to M into elements of the Lie algebra $\mathfrak{g}$ corresponding to G. Recall that elements in G correspond to translations and rotations of a body relative to its reference configuration. A vector tangent to G encodes instantaneous rates of change in position and orientation. Left-translating such a vector to the tangent space at the identity in G — in other words, into the Lie algebra $\mathfrak{g}$ — corresponds to mapping these instantaneous rates of change into the body frame.

If $A : TM \to \mathfrak{g}$ denotes the local connection form, then the requirement that a system evolve along horizontal trajectories is equivalent to the requirement that

$$\dot{g} + T_e L_g \left[A(r)\dot{r} \right] = 0. \tag{2.1}$$

This first term in this equation represents the rate of change of a body's position and orientation, and may be regarded as a column vector with height equal to the dimension of G. Within the square braces in the second term, the local connection form maps the rate of change of the body's shape into $\mathfrak{g}$ in a manner that depends on the shape r. Elements of the Lie algebra also correspond to column vectors with height equal to the dimension of G. The Lie algebra element $A(r)\dot{r}$ is mapped into the space in which $\dot{g}$ resides — the space tangent to G at the point g — through multiplication by the square Jacobian matrix $T_e L_g$ corresponding to left translation in G.

A common variation of (2.1) is obtained by prepending $(T_e L_g)^{-1}$ to each term, translating the objects they represent into $\mathfrak{g}$. We will invoke the symbol ξ for the *body velocity* $(T_e L_g)^{-1}\dot{g}$ in Sections 2.4 and 3.2.

The significance of (2.1) is that it separates the local connection form $A(r)$, which involves only shape variables, from aspects of the equations of motion that depend only on the group G. The equations governing the motion of any body relative to a spatially fixed frame of reference inherit significant complexity, in particular, when the body frame is able to rotate relative to the spatial frame. This complexity is generic to the choice of spatial frame, however, and is completely encoded in the matrix representing $T_e L_g$. The distinctions between two different kinematic systems for locomotion in the same ambient space — in other words, involving the

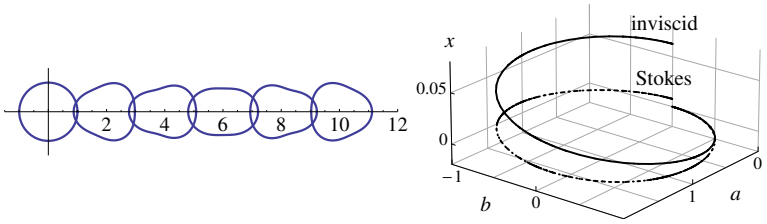

FIG. 2. *Driftless squirming locomotion. The panel on the left shows several snapshots of the locomotion of a massless cylinder with time-varying radius given by* (2.2)*, with* $(a, b) = (1 - \cos t, \sin t)$ *and* $\epsilon = 1/10$*, in an ideal flow. The snapshots depict the configuration of the cylinder at two-hundred-unit intervals in time. The panel on the right depicts the displacement of the cylinder throughout a single cycle of this gait in ideal flow and in Stokes flow. The panel on the right corresponds to Figure 1, with the* (a, b) *plane fibered by copies of the real line corresponding to the group* $(\mathbb{R}, +)$ *of translations in the x direction. The two curves correspond to horizontal lifts determined by different principal connections.*

same group G — are encoded entirely in the differences between the two local connection forms.

Note that (2.1) may be interpreted as a nonlinear control system in control-affine form, with the components of the column vector $\dot{r}$ viewed as control inputs. This system is *driftless* in the sense that no dynamics persist when the controls are equal to zero. In other words, (2.1) describes the locomotion of a body which instantly ceases to move if it ceases to deform. The controllability of (2.1), which depends only on the local connection form and the Lie bracket operation on $\mathfrak{g}$, is examined in [5].

2.3. Squirming Circles. We illustrate the constructions of Sections 2.1 and 2.2 with a pair of examples involving rectilinear swimming. Consider an evacuated circular cylinder with unit radius, initially centered about the origin in its cross-sectional plane, surrounded by a stationary incompressible fluid without no outer boundary. If the cylinder's profile is perturbed from circular in a time-varying way, it's possible for the cylinder to accelerate from rest.

Specifically, suppose the radius of the cylinder to be given, in body-fixed polar coordinates, by

$$r(t) = 1 + \epsilon \left(a(t) \cos 2\theta + b(t) \cos 3\theta \right). \tag{2.2}$$

If ϵ is a small parameter, we can use perturbation theory to determine the horizontal motion of the cylinder resulting from variations in the shape parameters a and b.

If the fluid is inviscid, the cylinder will translate such that

$$\dot{x} + \begin{bmatrix} -\epsilon^2 b & \epsilon^2 a \end{bmatrix} \begin{bmatrix} \dot{a} \\ \dot{b} \end{bmatrix} + O\left(\epsilon^3\right) = 0. \tag{2.3}$$

Compare this equation to (2.1). The group G comprises only translations in the x direction, and the Jacobian T_eL_g is the one-by-one identity matrix. The local connection form is represented (to order ϵ^2) by the matrix $[-\epsilon^2 b \quad \epsilon^2 a]$.

If Stokes flow is assumed instead of ideal flow, the cylinder will translate such that

$$\dot{x} + \begin{bmatrix} \frac{\epsilon^2 b}{4} & \frac{\epsilon^2 a}{2} \end{bmatrix} \begin{bmatrix} \dot{a} \\ \dot{b} \end{bmatrix} + O\left(\epsilon^3\right) = 0. \tag{2.4}$$

Figure 2 illustrates the difference between swimming in ideal flow and swimming in Stokes flow with a gait that favors the former. In either case, the displacement of the cylinder after a single cyclic deformation may be regarded as the *geometric phase* or *holonomy* associated with the corresponding closed path in the shape manifold with coordinates a and b.

The local connection form in (2.3) encodes the fact that the *Kelvin impulse* [8] in the system — effectively the total momentum — must remain zero even after the cylinder begins to deform, requiring that certain deformations be accompanied by translation. The conservation of impulse in the horizontal direction is equivalent, via *Noether's theorem* [9], to a one-dimensional symmetry manifest in the invariance of the system's kinetic energy under horizontal translations of the spatial frame of reference. Formally, we derive the local connection form — following a procedure outlined in [4] — by constructing the *momentum map* associated with this symmetry. In the context of the inviscid swimmer in Figure 2, the momentum map corresponds to the component of impulse in the horizontal direction, which is related to the left-hand side of (2.3) by a nonzero multiplicative factor.[1] The impulse, initially zero, is conserved if and only if the left-hand side of (2.3) equals zero.

This procedure applies to inviscid swimming in three dimensions as well, involving rotation as well as translation. In the most general case, the symmetry group is all of $SE(3)$, and the momentum map has six components corresponding to linear and angular impulse. The local connection form in this case — taking values in $\mathfrak{se}(3)$ — has six components as well, specifying the linear and angular velocity of the swimmer relative to the body frame such that all components of impulse remain zero.

Significantly, the same procedure is used to derive the local connection form governing locomotion in three-dimensional Stokes flow.[2] In this case, the relevant symmetry is the invariance not of the kinetic energy but of the rate of energy dissipation — the *Rayleigh dissipation function* — under translations and rotations of the spatial reference frame. Specifying that the corresponding momentum map remain zero is equivalent to specifying that the net force and moment on a swimmer remain zero in the low

[1] Specifically, the swimmer's effective mass in the horizontal direction.

[2] Planar Stokes flow requires a modified treatment due to *Stokes' paradox*[1].

Reynolds number limit, consistent with the negation of inertial phenomena by viscous effects.

2.4. Extensions to Systems with Drift. In certain cases, the notion of a connection on the bundle $M \times G$ over M may assist in the mathematical description of locomotion even when trajectories in M do not lift uniquely. Suppose, for instance, that a system is governed by Lagrange's equations subject to viscous dissipation, and that both the Lagrangian — generalizing the role played by kinetic energy in Section 2.3 — and the dissipation function are invariant under transformations in G. In such a case, a deforming body may accumulate momentum through cyclic deformation, translating or rotating to different degrees during successive cycles. The position and orientation of the body evolve dynamically in a manner coupled to the dynamics of the corresponding components of momentum.

If A_{mech} and A_{Stokes} denote the local connection forms derived from the Lagrangian and the dissipation function, respectively, then the dynamics of the system may be expressed in the form

$$\begin{aligned} \dot{g} &= T_e L_g \left(-A_{\text{mech}} \dot{r} + I^{-1} \, p \right) \\ \dot{p} &= V \left(A_{\text{Stokes}} - A_{\text{mech}} \right) \dot{r} + V I^{-1} \, p + \text{ad}^*_\xi \, p. \end{aligned} \tag{2.5}$$

Here p, a vector in the space $\mathfrak{g}^*$ dual to $\mathfrak{g}$, comprises the components of the momentum map derived from the Lagrangian — in other words, the linear and angular momentum or impulse — expressed in the body frame. If the momentum map is conserved, its representation in the body frame will change as the body frame does; the final term in the second line tracks this change. The *local locked inertia tensor* I expresses the body's shape-dependent inertia, and V the body's shape-dependent directional viscous resistance, in the body frame.

Observe that if $V = 0$ and if $p = 0$ initially — in other words, if all dissipation is removed from the system and the system is initially at rest — then (2.5) simplifies to (2.1) with A_{mech} as the local connection form. The significance of inertial effects relative to viscous effects is represented by IV^{-1}. Prepending this tensor term-by-term to the second line in (2.5) and letting $IV^{-1} \to 0$, we recover (2.1) with A_{Stokes} as the local connection form.[3]

Figure 3 depicts a system described by equations of the form (2.5). A simple walker with a uniformly dense elliptical body makes contact with the ground at four points, each at the end of a rigidly pivoting leg. The angles ϕ and ψ specify the shape of the walker as viewed from above. An additional parameter, representing the walker's ability to lift its legs in opposite pairs, specifies the distribution of the walker's weight on its four feet. Each foot is assumed to experience isotropic viscous resistance to sliding along the

[3]Compare the role of of IV^{-1} here to that of the Reynolds number in the Navier-Stokes equations, which become the equations for creeping flow as $Re \to 0$ [3].

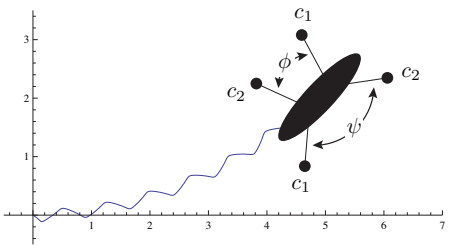

FIG. 3. *A quadrupedal walker governed by* (2.5)*, accelerating from rest. The gait shown corresponds to sinusoidal oscillations in* ϕ *and* ψ *that are exactly out of phase —* ψ *varies with a larger amplitude — overlaid with cosinusoidal oscillations in the balance between the effective viscous drag coefficients* c_1 *and* c_2*.*

ground; the effective damping coefficients c_1 and c_2 vary linearly with the normal forces applied to the ground by the feet. The path of the walker's center of mass is shown as it executes a shuffling gait defined by phased variations in leg position whereby no leg is ever completely unloaded.

A set of equations akin to (2.5), but representing the case in which inertial dynamics interact with nonholonomic constraints rather than dissipative forces, is developed in [2] in terms of the *nonholonomic momentum map* and *nonholonomic connection*.

3. Propulsion via Localized Discrete Vortex Shedding. Neither of the idealized models described in Section 2.3 captures the essential physics of fishlike swimming. The deficiency of both models is apparent in their time-reversibility. The undulation of a single rigid appendage will accelerate a macroscopic body from rest in water, yet the models from Section 2.3 prohibit the net displacement or reorientation of a swimmer as a result of cyclic variation in only one shape variable.[4]

Fishlike propulsion hinges on the interplay of inertial and viscous phenomena in a manner that also eludes the model from Section 2.4, which accommodates only those dynamic variables that directly represent the state of a self-propelling body. When a body moves through water, viscosity causes the water to adhere to the surface of the body, generating shear forces that might plausibly be modeled using the machinery of Section 2.4. Depending on the size and geometry of the body and its motion, however, the inertia of the water may prevent the flow from remaining attached at all points on the body. When a fluid flow separates from a body, vorticity is shed into the fluid and the body experiences a force reflecting the resulting momentum exchange. The vortical wake of a fishlike swimmer exhibits dynamics of its own, coupled to those of the swimmer itself but requiring independent accounting.

For the remainder of the paper, we focus on a model for planar swim-

[4] In the context of Stokes flow, this is the famous *scallop theorem* [13].

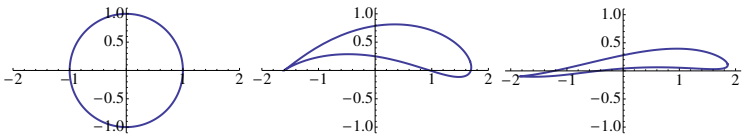

FIG. 4. *A circle in the complex plane and its images under Joukowski (center) and von Mises (right) transformations, both of the form* (3.1).

ming that seeks to encompass the central role played by vortex shedding in fishlike locomotion while sacrificing as little as possible of the mathematical structure present in the idealized models of Section 2. In fact, the geometric mechanics underpinning this model — a model involving the interaction of a free deforming body with a system of point vortices, with the number of vortices varying in a manner coupled to the time-varying circulation around the body — exhibits a richness beyond the scope of the present paper. We summarize features linking the model to its predecessors from Section 2, then proceed to a discussion of its dynamics. The model is detailed in [18].

3.1. Geometry and Modeling Assumptions. Figure 4 depicts a circle with radius $\varrho = 1$ in the complex ζ plane, centered about the origin, and its images under a pair of transformations of the form

$$z = (\zeta + \zeta_c) + \frac{a_1}{(\zeta + \zeta_c)} + \cdots + \frac{a_n}{(\zeta + \zeta_c)^n}. \tag{3.1}$$

Such transformations can be used to realize a variety of contours reminiscent of the profiles of practical airfoils [17]. Regarded as coordinates on a shape manifold, the radius ϱ and the real and imaginary parts of ζ_c and $a_1, \ldots, a_n$ may be varied periodically with time to specify the undulations of a planar swimmer.[5]

In particular, the first two panels in Figure 4 depict the *Joukowski transformation* obtained from (3.1) when $n = 1$ and a_1 is a positive real number. If ϱ is fixed, the imaginary part of ζ_c may be varied to realize variations in the camber of the resulting profile, while complementary variations in the real part of ζ_c and in a_1 preserve the area enclosed within. In the present paper, we focus on the self-propulsion of a Joukowski foil with a single internal degree of freedom corresponding to camber.

In the absence of vortex shedding, variations in a single shape parameter cannot accelerate a body through an ideal fluid if the system is initially at rest. The mechanism we introduce for vortex shedding from the Joukowski foil from Figure 4, however, enables the free foil to navigate from rest throughout the plane, so that $G = SE(2)$ in the language of Section 2.

[5]Our analysis relies on the use of conformal maps in the manner described in [11], prohibiting the arbitrary assignment of values to the parameters in (3.1). The conformal nature of the transformations used in our simulations is addressed in [18].

The body frame is affixed to the deforming foil so that its coordinate axes coincide with the real and imaginary axes of the complex plane in which the foil's shape is obtained from the Joukowski map.

Adopting the perspective of [16] and significant subsequent literature, we focus on vortex shedding from the sharp trailing tip of the foil — modeling the caudal fin of a fish viewed in cross-section — as a mechanism for propulsion. We assume the fluid surrounding the foil to be ideal, and confine the representation of viscous phenomenology to the time-periodic enforcement of a *Kutta condition* [3] at this single point.

The Kutta condition compels smooth flow separation from the foil's trailing tip by requiring that the preimage of the tip in the ζ plane correspond to a stagnation point for the preimage of the flow. This condition can be enforced continuously through the continuous introduction of vorticity to the fluid, but we amend the flow only at regular instants in time by introducing discrete vortices near the foil's tip. Given the freedom to choose both the location and the strength of a newly introduced vortex, we can enforce the Kutta condition in more than one way. The simulations depicted below rely on a method adapted from [15] whereby the location of each new vortex is specified before its strength, and shed vortices need not have the same strength. A comparison of alternate methods appears in [18]. Once shed, each vortex in our model remains constant in strength.

New vortices are introduced to the fluid in a manner that respects two conservation laws, each of which can be traced to a symmetry of the fluid-foil system. Consistent with *Kelvin's circulation theorem* [3], the circulation around the foil changes discretely with the shedding of each new vortex to ensure that the circulation around any contour enclosing the foil and its wake remain zero. Changes in the circulation around the foil may be attributed to the introduction of *image vortices* [11] within the foil. The relationship between Kelvin's theorem and the invariance of kinetic energy under fluid particle relabeling is discussed in [10].

Consistent with the conservation of total impulse in the system, the linear and angular momenta of the foil must also change discretely with the introduction of each new vortex. Note that changes in the foil's velocity affect the fluid velocity, requiring the simultaneous application of the constraints imposed on shed vortex strength and placement by the Kutta condition and by impulse conservation.

3.2. Hamiltonian Structure. The interaction of a free solid body with a finite collection of point vortices in an infinite ideal fluid is governed by a system of ordinary differential equations exhibiting a non-canonical Hamiltonian structure. This is demonstrated in [14] for the case in which the body is rigid. We summarize the extension in [18] to the case in which the body deforms as the image of a circle with radius ϱ, centered about the origin in the complex ζ plane, under a time-varying transformation $z = F(\zeta)$. We assume $z = F(\zeta)$ to be parametrized by coordinates r_j

on the appropriate shape manifold. Between vortex-shedding events, the swimming foil in our model interacts with ambient vortices — whether previously shed by the foil or present initially — according to these equations.

The phase space in question is the product of $\mathfrak{g}^*$ — elements p in which encode the linear and angular impluse in the system — and the space of coordinate pairs (x_i, y_i) specifying the positions of the vortices relative to the body frame. If n denotes the total number of vortices at a given time and γ_i the strength of the ith vortex, we may define a Hamiltonian of the form

$$H(p, x_1, y_1, \ldots, x_n, y_n) = H_0 - 2\pi H_1 \tag{3.2}$$

relative to which the fluid impulse evolves according to the *Lie-Poisson equation*

$$\dot{p} = \mathrm{ad}^*_{\delta H/\delta p}\, p$$

and the positions of the vortices evolve according to the equations

$$-2\pi\gamma_i \dot{x}_i = \frac{\partial H}{\partial y_i}, \qquad -2\pi\gamma_i \dot{y}_i = -\frac{\partial H}{\partial x_i}.$$

The significance of the Lie-Poisson equation in Hamiltonian mechanics is detailed in [9].

While expressible in terms of the phase variables named above, the first term in the Hamiltonian (3.2) is most easily understood as

$$H_0 = \frac{1}{2}\xi^T I \xi,$$

where ξ and I are the body velocity vector and locked inertia tensor from Section 2. The second term in the Hamiltonian is proportional to

$$\begin{aligned} H_1 = &\sum_i \gamma_i \sum_j \dot{r}_j \psi_j(x_i, y_i) - \frac{1}{2}\sum_i \gamma_i^2 \left(\log\left|\zeta_i\bar{\zeta}_i - \varrho^2\right| + \log\left|F'(\zeta_i)\right|\right) \\ &+ \frac{1}{2}\sum_i \sum_{i\neq j} \gamma_i\gamma_j \left(\log|\zeta_i - \zeta_j| - \log\left|\zeta_k\bar{\zeta}_j - \varrho^2\right|\right), \end{aligned}$$

where ζ_i denotes the preimage of the location of the ith vortex in the ζ plane and $\dot{r}_j\psi_j$ is the component of the stream function in the ζ plane due to variations in the shape parameter r_j.

3.3. Steady Swimming. Vortex shedding from the trailing tip of a free Joukowski foil serves to rectify oscillations in the foil's camber to generate locomotion. Figure 5 depicts snapshots from simulations of three different swimming gaits corresponding to different cyclic variations in camber over time. The foil begins at rest and oscillates at the same frequency

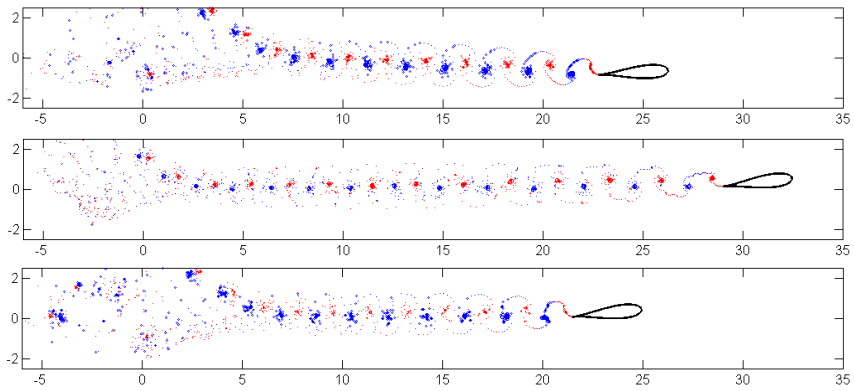

FIG. 5. *Three different swimming gaits for the Joukowski foil. As a function of time, the rate of change of the camber parameter $r(t)$ is a sine wave in the top panel, a square wave in the middle panel, and a triangle wave in the bottom panel.*

in each case, and the three snapshots depict the same instant in time. Shed vortices appear as dots in the foil's wake, scaled according to strength and shaded according to sign. In all three cases shown, the emergence of steady swimming corresponds to the development of the wake structure depicted in [16] — an *inverse Kármán vortex street* — comprising rolled-up collections of vortices of alternating sign.

The sole input to the model is the rate of change $\dot{r}$ of the point in the shape manifold corresponding to the foil's camber. The three gaits shown have been normalized so that the integral of $|\dot{r}|^2$ over one period of oscillation, roughly measuring economy of deformation, is the same in each case. Persistent oscillations in camber always drive the foil toward steady rectilinear swimming, but the asymptotic swimming speed and the detailed structure of the steady-state wake vary from gait to gait.

4. Locomotion Under Heading Control. Among the authors' motivations for developing an idealized model for fishlike swimming is the prospect of using the model as a platform for developing control strategies for a fishlike robotic vehicle. In the remaining pages, we outline a simple approach to the control of the swimming Joukowski foil.

The swimming foil may be viewed as a control system with $\dot{r}$ as the input and the position and orientation of the foil relative to a spatially fixed frame of reference — collectively, an element of $SE(2)$ — as outputs. The *underactuated* nature of this system presents a significant challenge; the desire for the foil to navigate using bounded, cyclic changes in shape complicates the problem further.

Figure 6 demonstrates that the orientation of the foil can be controlled using feedback. The foil is at rest initially, oriented with no relative rotation between the body frame and the spatial frame. We refer to the angle

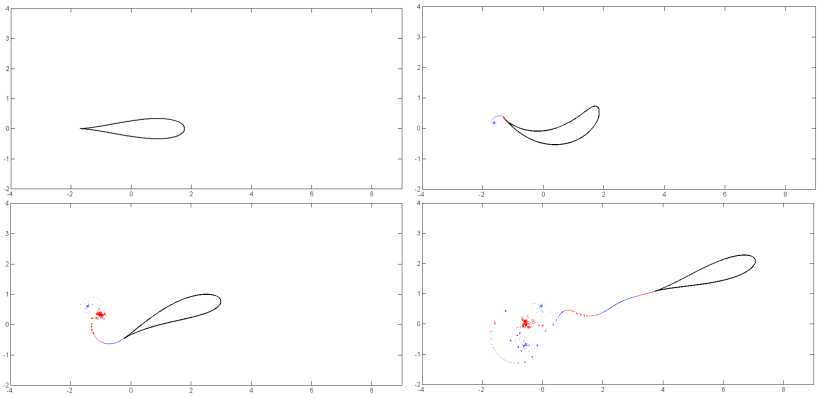

FIG. 6. *A .3-radian turn executed from rest using PID control to vary the camber of the foil as a function of the error between its current heading and the desired heading.*

between the two frames as the foil's *heading*, and specify a desired heading as a function of time. We denote the discrepancy between the desired heading and the actual heading as $\varepsilon(t)$ and implement a standard *PID controller* such that

$$\dot{r}(t) = k_p\varepsilon(t) + k_i \int_0^t \varepsilon(\tau)d\tau + k_d\dot{\varepsilon}(t). \tag{4.1}$$

Constant values can be assigned to k_p, k_i, and k_d — respectively, the *proportional*, *integral*, and *derivative gains* — to realize closed-loop systems with different dynamic properties.

Figure 6 depicts snapshots of the foil's response to an abrupt change in the desired heading from 0 to .3 radians. The controller gains have been chosen so that oscillations in the heading about the desired value decay over time. As a result of the maneuver, $\varepsilon(t)$ approaches zero asymptotically and the foil settles into a steady coast in the desired direction.

4.1. Single-Input Planar Navigation. Experiments indicate that large step changes in the desired heading of the foil can be tracked with no steady-state error using a variety of different controller gains. In particular, a purely proportional controller obtained by setting $k_i = k_d = 0$ in (4.1) is generally sufficient to guarantee that the foil's time-averaged heading will tend to the desired value, though oscillations in the foil's camber, and thus in the instantaneous heading, may persist in this case.

Under purely proportional control, the average translational speed of the foil as it completes its response to a step change in desired heading varies with the value of the proportional gain k_p. This is illustrated in Figure 7, which shows the foil responding to such a step change alongside a plot of the foil's forward speed — in other words, the component of velocity in the body-fixed positive x direction — versus time for different choices

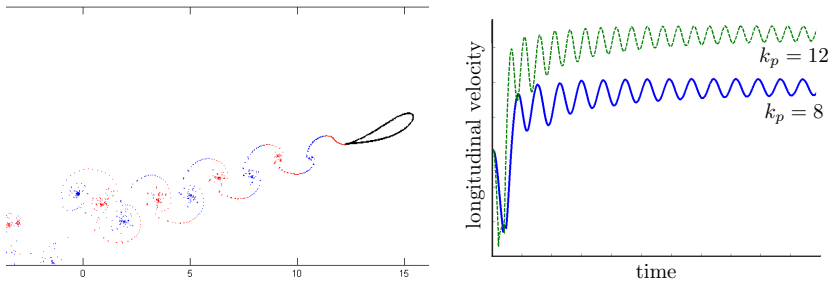

FIG. 7. Left: *A directional change under proportional heading control, leading to steady average translation at a speed determined by the proportional gain* k_p. Right: *The longitudinal velocity of the foil as it executes such a maneuver, as a function of time, for two different values of* k_p.

of k_p. The foil begins not at rest but coasting steadily from left to right, parallel with the bottom of the figure.

Proportional heading control thus forms the basis for a simple method whereby the foil can navigate throughout the plane. Desired changes in swimming direction are achieved through feedback between heading and camber; changes in the steady-state swimming speed are achieved through changes in the feedback gain.

4.2. Energy Harvesting. A nonzero background flow can complicate the variations in camber required for the foil to track a desired heading, but need not increase the control effort required to attain a desired heading and asymptotic speed. Figure 8 illustrates the use of PID control for *energy harvesting* from an array of vortices corresponding to the fully rolled-up wake of a foil executing the sinusoidal gait from Figure 5.

The controller gains are chosen to damp oscillations in the foil's camber and the desired heading remains equal to the foil's initial heading. As the ambient vortices begin to rotate the foil, it responds in a manner that stabilizes its motion through the middle of the street. Without deformation, the foil would be ejected laterally [6]. With control, it attains a translational kinetic energy greater than that achievable with the same economy of deformation in a quiescent fluid, while the total *interaction energy* [12] among vortices decreases.

REFERENCES

[1] G. Birkhoff, *Hydrodynamics: A Study in Logic, Fact, and Similitude*, Greenwood Publishing Group, 1978.

[2] A. M. Bloch, P. S. Krishnaprasad, J. E. Marsden, and R. M. Murray, *Nonholonomic Mechanical Systems with Symmetry*, Archive for Rational Mechanics and Analysis **136** (1996), 21–99.

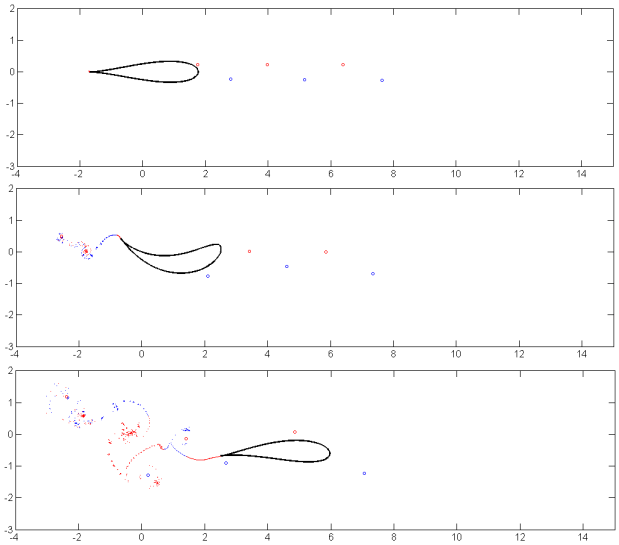

FIG. 8. *Drafting the wake of a preceding foil via PID control.*

[3] S. Childress, *Mechanics of Swimming and Flying*, Cambridge University Press, 1981.

[4] S. D. Kelly, *The Mechanics and Control of Robotic Locomotion with Applications to Aquatic Vehicles*, Ph.D. thesis, California Institute of Technology, 1998.

[5] S. D. Kelly and R. M. Murray, *Geometric Phases and Robotic Locomotion*, Journal of Robotic Systems **12** (1995), 417–431.

[6] S D. Kelly and P. Pujari, *Propulsive Energy Harvesting by a Fishlike Vehicle in a Vortex Flow: Computational Modeling and Control*, Proceedings of the 49th IEEE Conference on Decision and Control, 2010.

[7] S. Kobayashi and K. Nomizu, *Foundations of Differential Geometry*, vol. 1, Interscience Publishers, 1963.

[8] Sir H. Lamb, *Hydrodynamics*, Dover, 1945.

[9] J. E. Marsden and T. S. Ratiu, *Introduction to Mechanics and Symmetry*, 2nd ed., Springer-Verlag, 1999.

[10] J. E. Marsden and A. Weinstein, *Coadjoint Orbits, Vortices, and Clebsch Variables for Incompressible Fluids*, Physica 7D (1983), 305–323.

[11] L. M. Milne-Thomson, *Theoretical Hydrodynamics*, Dover, 1996.

[12] P. K. Newton, *The N-Vortex Problem*, Springer-Verlag, 2001.

[13] E. Purcell, *Life at Low Reynolds Number*, American Journal of Physics **45** (1977), 3–11.

[14] B. N. Shashikanth, *Poisson Brackets for the Dynamically Interacting System of A 2D Rigid Cylinder and N Point Vortices: the Case of Arbitrary Smooth Cylinder Shapes*, Regular and Chaotic Dynamics **10** (2005), no. 1, 1–14.

[15] K. Streitlien and M. S. Triantafyllou, *Force and Moment on a Joukowski Profile in the Presence of Point Vortices*, AIAA Journal **33** (1995), no. 4, 603–610.

[16] T. von Kármán and J. M. Burgers, *General Aerodynamic Theory: Perfect Fluids*, Aerodynamic Theory, vol. II, Springer-Verlag, 1934.

[17] R. von Mises, *Theory of Flight*, Dover, 1959.

[18] H. Xiong, *Geometric Mechanics, Ideal Hydrodynamics, and the Locomotion of Planar Shape-Changing Aquatic Vehicles*, Ph.D. thesis, University of Illinois at Urbana-Champaign, 2007.